

A PDTPQx:PC61BM blend with pronounced charge-transfer absorption for organic resonant cavity photodetectors – direct arylation polymerization vs. Stille polycondensation

Peer-reviewed author version

VANDERMEEREN, Tom; LIU, Quan; GIELEN, Sam; THEUNISSEN, Dries; FREDERIX, Siebe; VAN LANDEGHEM, Melissa; Liu, Zhen; Van den Brande, Niko; D'HAEN, Jan; VANDERSPIKKEN, jochen; LUTSEN, Laurence; VANDEWAL, Koen & MAES, Wouter (2022) A PDTPQx:PC61BM blend with pronounced charge-transfer absorption for organic resonant cavity photodetectors – direct arylation polymerization vs. Stille polycondensation. In: *Dyes and Pigments*, 200 (Art N° 110130).

DOI: 10.1016/j.dyepig.2022.110130

Handle: <http://hdl.handle.net/1942/36853>

A PDTPQx:PC₆₁BM Blend with Pronounced Charge-Transfer Absorption for Organic Resonant Cavity Photodetectors – Direct Arylation Polymerization vs. Stille Polycondensation

Tom Vandermeeren^{a,b,c}, Quan Liu^{a,b,c}, Sam Gielen^{a,b,c}, Dries Theunissen^{a,b,c}, Zhen Liu^d, Niko Van den Brande^d, Jan D'Haen^{a,b,c}, Jochen Vanderspikken^{a,b,c}, Laurence Lutsen^{a,b,c}, Koen Vandewal^{a,b,c}, Wouter Maes^{a,b,c,*}

^a Hasselt University, Institute for Materials Research (IMO), Agoralaan Building D, 3590 Diepenbeek, Belgium

^b IMEC, Associated Lab IMOMECE, Wetenschapspark 1, 3590 Diepenbeek, Belgium

^c Energyville, Thorpark, 3600 Genk, Belgium

^d Vrije Universiteit Brussel, Physical Chemistry and Polymer Science, Pleinlaan 2, 1050 Brussels, Belgium

* Corresponding author. E-mail address: wouter.maes@uhasselt.be

Keywords: direct arylation polymerization; organic photodetectors; near-infrared; intermolecular charge transfer; optical cavities

Abstract. Because of their intriguing properties for optoelectronic applications, research on organic semiconducting polymers has steadily progressed over the past decades, yielding increasingly fine-tuned (hetero)aromatic polymer backbones. In this work, the push-pull copolymer PDTPQx is synthesized, both *via* Stille polycondensation and direct arylation polymerization (DARp), permitting comparison of the two procedures. Near-infrared organic photodetectors (OPDs) are constructed based on these different polymer batches in combination with PC₆₁BM, and their performance was investigated. From the current-voltage characteristics, it is clear that the DARp polymer-based devices outperform those prepared from the Stille polymers, both in terms of dark current density and external quantum efficiency (EQE), and therefore in terms of specific detectivity as well. The relatively high highest occupied molecular orbital energy level of PDTPQx, in combination with the clear charge-transfer absorption band observed for the DARp-based device, is beneficial for application in organic resonant cavity photodetectors. Such OPDs are prepared for the DARp PDTPQx:PC₆₁BM (1:4) blends with 180 and 210 nm thick bulk heterojunction active layers. EQEs of 2.5% at 1016 nm and 1% at 1140 nm are achieved, with full-width-at-half-maximum peak responses of 44 and 45 nm, respectively, and detectivities of 2.24×10^{10} and 1.06×10^{10} Jones.

1. Introduction

Light-based technology has become one of the pillars of our digital society. The quest for new and innovative electronics continues to grow. In order to keep up with this ever-increasing need, the design of new as well as the optimization of known materials is required. Organic semiconducting polymers have attracted much attention due to their potential applications in flexible and wearable electronics. They show inherent softness, flexibility, low weight, adjustable optoelectronic properties through tailored design of the molecular structure, and low-cost, large-scale production possibilities.¹ The versatility of synthetic organic and polymer chemistry enables these materials to be tuned as such that they can be incorporated into diverse optoelectronic devices,² such as organic photovoltaics (OPVs)³, organic light-emitting diodes (OLEDs)⁴, organic photodetectors (OPDs)^{5, 6} and organic field-effect or electrochemical transistors (OFETs or OECTs)^{7, 8}, emphasizing the role of chemical design in the performance of organic semiconductors.⁹ Increasingly fine-tuned (hetero)aromatic polymer backbones are being explored as a consequence of their interesting properties, advancing research on

organic semiconducting polymers. Therefore, also the demand for convenient, reliable, and efficient synthetic routes toward these polymer backbones has increased.

High-performance π -conjugated polymers with well-defined structures are typically synthesized via a transition metal-catalyzed cross-coupling polycondensation such as Migita-Kosugi-Stille¹⁰, Suzuki-Miyaura¹¹, Kumada-Corriu¹² and Negishi¹³, amongst others. Although these cross-coupling reactions necessitate the functionalization of both coupling sites, they have developed into effective synthetic protocols for organic and polymer chemistry. Metal-promoted C–H activation toward C–C bonds has been changing the field of synthetic chemistry for over half a century now,¹⁴ yet it has only recently been explored for the synthesis of π -conjugated polymers, a procedure more widely known as direct arylation polymerization (DAP). This protocol requires the pre-activation of only one coupling site (*i.e.* the aryl halide), circumventing the preparation of organometallic derivatives and the associated cryogenic air- and water-free reaction conditions,¹⁵ yielding a major two-fold advantage. First, the material synthesis is significantly simplified, in this way potentially enabling to use monomers that are not compatible with organometallic functionalization.¹⁵ Second, it further solidifies the position of organic electronics as less toxic, more environmentally friendly, and more sustainable than their inorganic counterparts.¹⁶⁻¹⁸ Furthermore, DAP appeals for its atom economy, effectiveness (providing targets in fewer synthetic steps), generation of more benign byproducts, and decrease of the overall cost for the preparation of conjugated polymers.

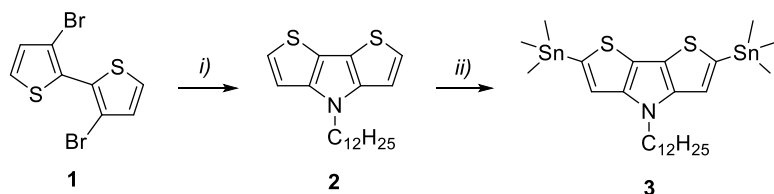
Although a broad range of monomers are now readily polymerizable,¹⁵ DAP is known to produce defects in the chemical structure. For instance, the reactivity of C–H bonds on (hetero)aromatic β -carbon atoms can result in branched or cross-linked polymer chains. This is often countered by using a low-dielectric solvent (for instance toluene, xylenes or tetrahydrofuran) to yield low-defect materials.¹⁴ As for other metal-catalyzed cross-coupling polymerizations, also for DAP homocoupling is a factor to take into account.¹⁴ All of these defects have a significant effect on the optical and electronic properties of conjugated polymers.¹⁹⁻²¹ Although some fundamental understanding of different DAP reaction protocols has been established, more detailed insights will be required to truly enable a broad reach within the field of organic electronics.

In this work, the donor-acceptor type copolymer PDTPQx is synthesized. The electron-rich dithieno[3,2-*b*:2',3'-*d*]pyrrole (DTP) unit is a small ladder-type moiety commonly employed in conjugated organic oligomers and polymers for organic electronics.²²⁻²⁶ On the other hand, the electron-poor quinoxaline (Qx) core is generally known for its easily modifiable structure, allowing to tune the electrical, optical, and morphological properties for both polymers and small molecules.²⁷ The combination of both units affords the unique PDTPQx polymer with a high highest occupied molecular orbital (HOMO) energy level. The polymer is synthesized both *via* Stille polycondensation and DAP, permitting an interesting comparison of the two. The high-HOMO characteristic of PDTPQx is desired for its application in organic resonant cavity photodetectors, as this decreases the energy of the intermolecular charge-transfer (CT) absorption of the polymer:PC₆₁BM blend, with a concomitant redshift of the direct CT absorption into the near-infrared (NIR).^{6, 28-31} Therefore, the DAP PDTPQx:PC₆₁BM blend is well suited to implement into a resonant optical cavity device architecture. Using this type of OPD, wavelength selective photodetection up to 1140 nm is achieved.

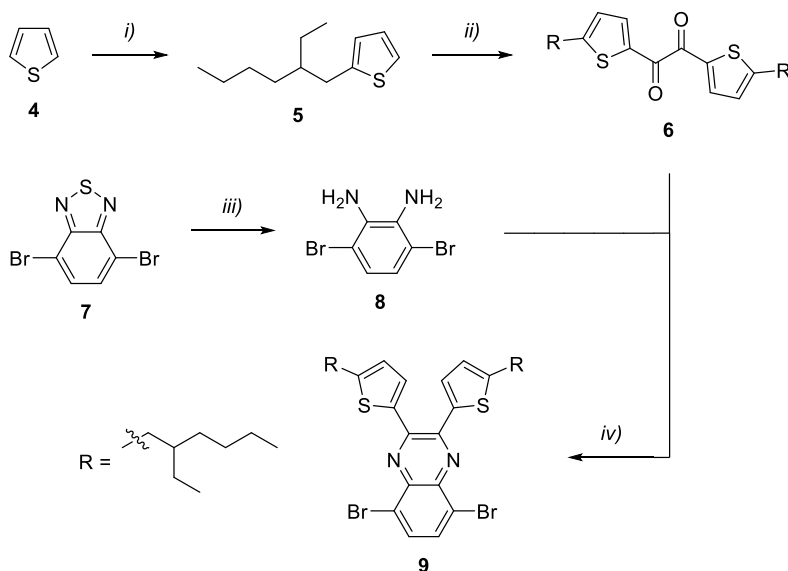
2. Results and discussion

The DTP synthesis (**Scheme 1**) starts with the Buchwald-Hartwig amination cyclization reaction of the commercially available 3,3'-dibromo-2,2'-bithiophene (**1**) with dodecylamine. The long *N*-alkyl side chain on the DTP unit ensures good solubility of the intended polymer. Stannylation using *n*-butyllithium and trimethyltin chloride generates the distannylated DTP monomer **3**.³² The quinoxaline

synthesis (**Scheme 2**) starts with the alkylation of thiophene with 2-ethylbromohexane, providing the alkylated thiophene **5**. Next, a Friedel-Crafts acylation with oxalyl chloride is performed, producing diketone **6**. Parallel to these reactions, 4,7-dibromobenzo[*c*][1,2,5]thiadiazole is reduced to its corresponding diamine using sodium borohydride. Diamine **8** is condensed with diketone **6**, yielding the desired bromine flanked quinoxaline monomer **9**.³³



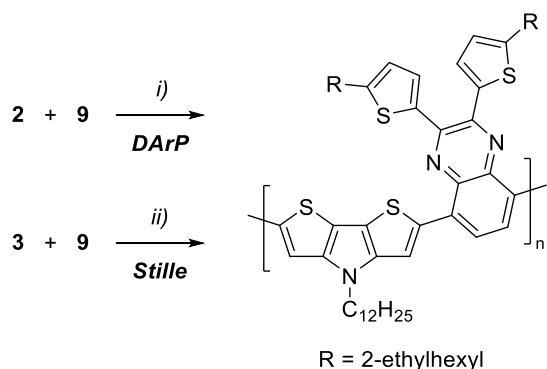
Scheme 1 Synthesis steps toward 4-dodecyl-2,6-bis(trimethylstannyl)-4*H*-dithieno[3,2-*b*:2',3'-*d*]pyrrole (**3**): *i*) dodecylamine, Pd₂(dba)₃, BINAP, sodium *tert*-butoxide, toluene, 120 °C (84%); *ii*) *n*-butyllithium, trimethyltin chloride, THF, -78 °C to RT (65%).



Scheme 2 Synthesis steps toward 5,8-dibromo-2,3-bis(5-(2-ethylhexyl)thiophen-2-yl)quinoxaline (**9**): *i*) *n*-butyllithium, KI, 2-ethylbromohexane, diethyl ether, -78 °C to RT (20%); *ii*) oxalyl chloride, AlCl₃, pyridine, dichloromethane, -20 °C to RT (24%); *iii*) NaBH₄, ethanol, RT (51%); *iv*) *p*-toluenesulfonic acid, methanol, reflux (73%).

The quinoxaline monomer **9** is then copolymerized with DTP monomers **2** and **3** *via* DArP and Stille polycondensation, respectively, yielding PDTPQx, as shown in **Scheme 3**. Two batches of PDTPQx are prepared *via* Stille polycondensation, referred to as 'Stille-L' and 'Stille-H' for the lower and higher molar mass batch, respectively. The only synthetic difference between the batches is the reaction time used and the amount of the catalytic system added. The PDTPQx batch prepared *via* DArP will simply be referred to as 'DArP'. The direct arylation polymerization reaction conditions are based on conditions reported by the Ozawa group, which were shown to inhibit branching and cross-linking.³⁴ All detailed reaction conditions are described in the supporting information (SI). All copolymers are

purified by successive Soxhlet extractions, supplying the largest amounts from the dichloromethane fraction, indicating a high solubility of the PDTPQx polymers.



Scheme 3 Synthesis steps toward PDTPQx *via* direct arylation polymerization (DArP) (i) and Stille polycondensation (ii): i) Pd₂(dba)₃, tris(*o*-anisyl)phosphine, Cs₂CO₃, pivalic acid, TMEDA, toluene, 100 °C; ii) Pd₂(dba)₃, tri(*o*-tolyl)phosphine, toluene:DMF (4:1), 120 °C.

All copolymers are then analyzed by high-temperature gel permeation chromatography (HT-GPC; **Figure S7**), yielding their molar masses and dispersities (\mathcal{D}), shown in **Table 1**. The Stille-L and Stille-H batches have number average molar masses (M_n) of 12.7 and 27.1 kg mol⁻¹ respectively, while the DArP fits right in between with a value of 19.9 kg mol⁻¹. Dispersities in the range of 2.2 to 2.6 are obtained. Cyclic voltammetry (CV) measurements are performed to estimate the frontier molecular orbital energy levels of the polymers (**Figure S8**). As expected, consistent energy level values are observed for all polymer samples, around -3.2 and -4.8 eV for the LUMO (lowest unoccupied molecular orbital) and HOMO, respectively. This is confirmed by the UV-Vis-NIR absorption spectra of the materials, where all peak maxima are situated within an 8 nm range from 752 nm, in solution and in film (**Figure 1**). The thermal properties of all polymer batches are studied *via* thermogravimetric analysis (TGA) and rapid heat-cool calorimetry (RHC). Mass loss is observed from *ca.* 400 °C for all polymer batches *via* TGA (**Figure S9**). RHC shows a very small melting peak for each polymer (**Figure S10**), even after using a cooling rate of 20 K min⁻¹ to promote crystallization upon cooling, which exhibits a dependence on molar mass. Values for the peak maximum of the melting transition (T_m) and the melting enthalpy (ΔH_m) can be found in **Table 1**. For the lowest molar mass polymer Stille-L, the highest ΔH_m is observed, as well as a clearly broader melting peak with a more pronounced low-temperature contribution, and a lower T_m . The melting behavior of the Stille-H and DArP polymers is more similar, with a higher T_m for the higher molar mass Stille-H, and only a small difference in ΔH_m , indicating a similar degree of crystallinity. The observed dependence of melting behavior on molar mass may correspond to classical polymer crystallization, where extended chain crystals are formed at low molar mass and chain folding occurs at higher molar mass, as seen for *e.g.* poly(3-hexylthiophene).³⁵

Table 1 Overview of the PDTPQx characterization data.

Polymer	M_n^a (kg mol ⁻¹)	\mathcal{D}^a	$\lambda_{\max, \text{film}}^b$ (nm)	E_{red}^c (V)	E_{ox}^c (V)	E_{LUMO}^d (eV)	E_{HOMO}^d (eV)	$E_{g, \text{opt}}^e$ (eV)	$E_{g, \text{CV}}^f$ (eV)	T_m^g (°C)	ΔH_m^h (J g ⁻¹)
Stille-L	12.7	2.2	756	-1.68	-0.12	-3.22	-4.77	1.43	1.56	213	3.9
Stille-H	27.1	2.3	756	-1.67	-0.10	-3.22	-4.79	1.44	1.56	239	2.5
DArP	19.9	2.6	749	-1.67	-0.10	-3.23	-4.79	1.42	1.57	228	2.4

^a Measured by HT-GPC at 160 °C in 1,2,4-trichlorobenzene. ^b Films were prepared by drop-casting a solution of the polymer onto a quartz disc. ^c Onset potentials vs. Fc/Fc⁺. ^d Determined from the onset of oxidation/reduction in CV. ^e Optical bandgap,

determined by the onset of the solid-state UV-Vis-NIR spectrum. ^f Electrochemical bandgap. ^g Melting transition peak maximum. ^h Melting enthalpy.

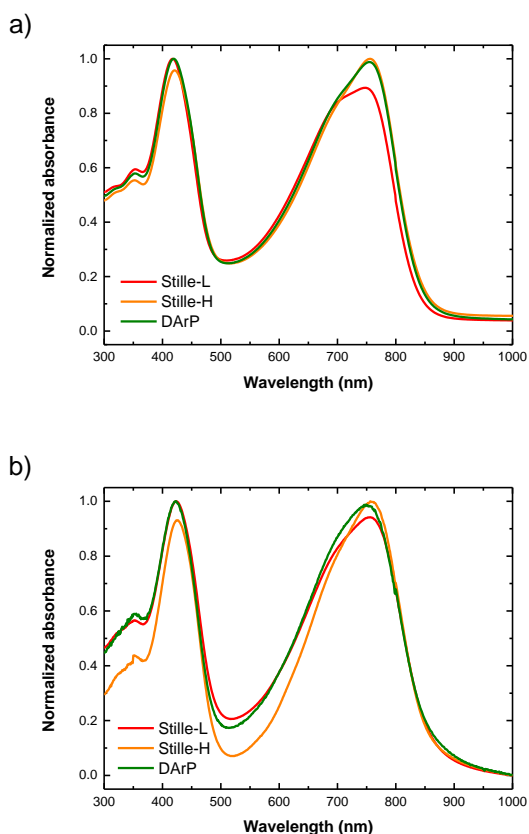
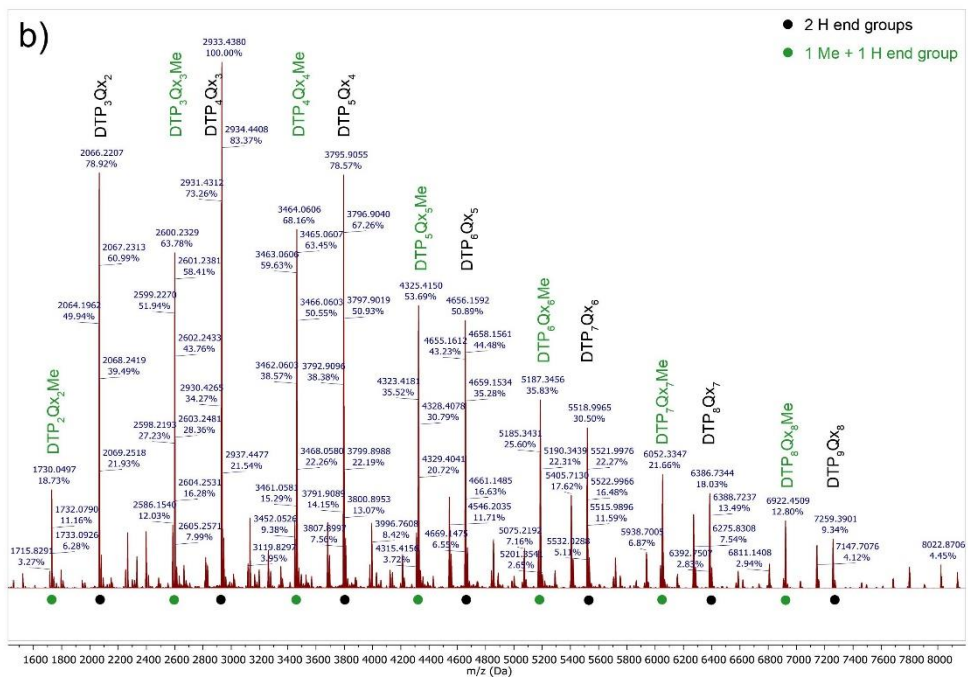
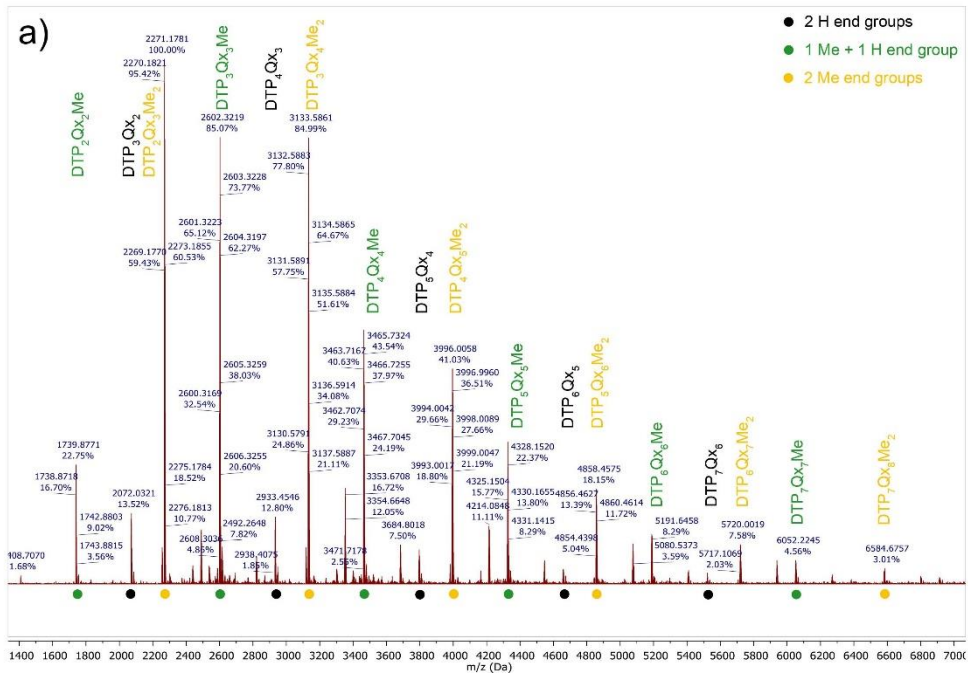


Figure 1 UV-Vis-NIR absorption spectra of PDTPQx in (a) solution and (b) drop-casted film.

The polymer structures are investigated in more detail *via* proton nuclear magnetic resonance (¹H-NMR) in *ortho*-dichlorobenzene-*d*₄ at 110 °C (**Figure S4-S6**). No major differences are observed between the polymers, except for somewhat better resolved signals for the lowest molar mass sample Stille-L. Therefore, matrix-assisted laser desorption/ionization - time-of-flight (MALDI-ToF) mass spectrometry is additionally applied (**Figure 2**). For all polymer batches, no mismatch in the amount of DTP and Qx building blocks is observed, pointing toward little or no homocoupling. In both Stille batches, the polymers show hydrogen, methyl, or both end groups. The methyl end groups are known to originate from the trimethylstannyl functionalization of the Stille monomer.²⁰ The DArP batch shows a main distribution with hydrogen end groups, but also two smaller distributions, either with one bromine or one tolyl end group. The major difference between the Stille and DArP polymers hence seems to be in their molar mass and end groups. Although the used DArP conditions should limit branching and cross-linking, this cannot be fully excluded either.³⁴



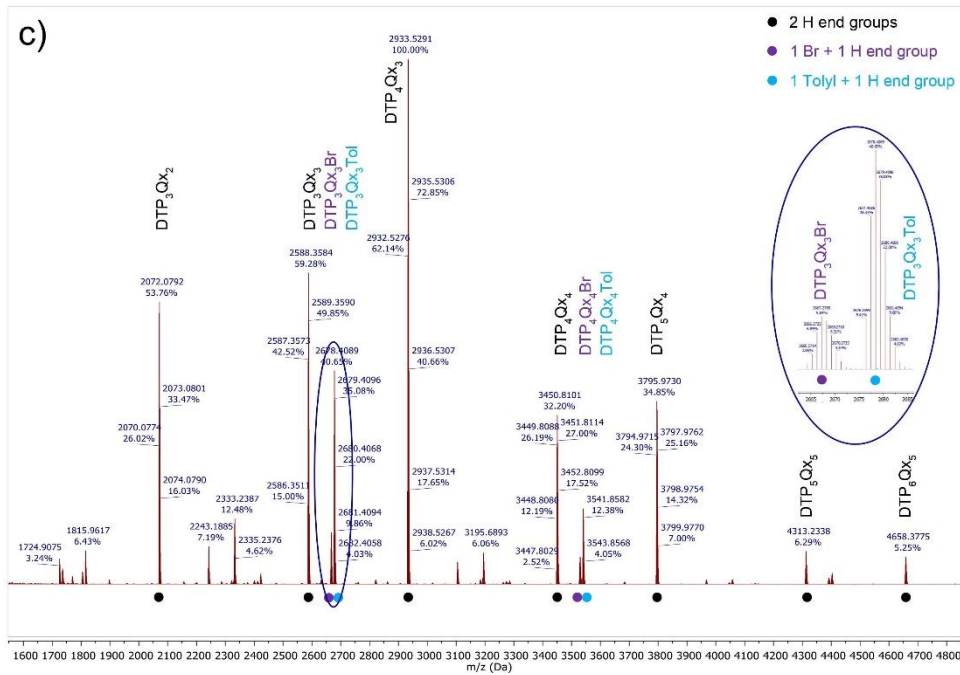


Figure 2 MALDI-ToF mass spectra of (a) the Stille-L PDTPQx polymer, (b) the Stille-H PDTPQx polymer, and (c) the DARp PDTPQx polymer (with a zoom-in of the m/z region from 2665 to 2685 Da).

To assess possible influences of the synthesis protocol on the materials performance in OPDs, bulk heterojunction (BHJ) blends of all polymers with PC₆₁BM are analyzed in the inverted photodiode stack ITO/PEIE/PDTPQx:PC₆₁BM/MoO₃/Ag. Sample preparation, OPD fabrication, optimization, and characterization details can be found in the SI. First, the optimal PDTPQx:PC₆₁BM ratio is determined. The 1:4 ratio affords the best results based on the dark current density (J_D) and external quantum efficiency (EQE) (**Figure S11**), and is therefore used in further optimizations. Second, optimization of the processing conditions for the Stille and DARp PDTPQx:PC₆₁BM (1:4) blends is performed, for which the data can be found in **Figure S12-S14**. The best overall results are achieved when the active layer blend is spin-coated from chloroform with the solvent additive 1,8-diiodooctane (DIO; 5 v/v%). For all optimized devices, the current density–voltage ($J - V$) characteristics under dark (J_D) and illuminated conditions are shown in **Figure 3a**. A low J_D and a high EQE are crucial in achieving a high-efficiency photodetector with a high specific detectivity (D^*). Both Stille batches afford a significantly higher dark current than the DARp polymer in the reverse biased region, where the OPD normally operates. The difference in J_D is about two orders of magnitude at -2 V. **Figure 3b,c** shows the EQE of all optimized devices in a linear and logarithmic plot, respectively. Fourier-transform infrared (FTIR) spectroscopy is used to sensitively measure the EQE spectrum, which is plotted on a logarithmic scale in **Figure 3c**. Only for the DARp PDTPQx-based blend, a pronounced CT absorption band is present between 950 and 1150 nm. This suggests the blends differ in energetic landscape at the donor:acceptor interface, which might explain the difference in J_D and EQE. Eventually, the calculated D^* at -0.1 and -2 V is plotted in **Figure 3d** for all optimized devices (**Table S1**). Due to the high dark currents obtained with the Stille polymer batches, their EQE spectra at -2 V could not be measured as the signal is dominated by noise. Therefore, no D^* at -2 V is calculated for Stille-L and Stille-H. For the calculation of D^* at -0.1 V, both shot and thermal noise are taken into account, applying the more general equation for the specific detectivity (expressed in $\text{cm Hz}^{1/2} \text{W}^{-1}$ or Jones):

$$D^* = \frac{q\lambda EQE}{hc \sqrt{\frac{4k_B T}{R_{sh}} + 2qJ_D}} \quad (1)$$

with q the elementary charge, λ the wavelength at which the EQE is measured, B the bandwidth of the photodetector, h Planck's constant, c the speed of light, k_B the Boltzmann constant, and R_{sh} the shunt resistance (derived from J_D at -0.1 V). At -2 V, OPDs are shot noise limited ($4k_B T/R_{sh} \ll 2qJ_D$), simplifying the equation of D^* :

$$D^* = \frac{q\lambda EQE}{hc\sqrt{2qJ_D}} \quad (2)$$

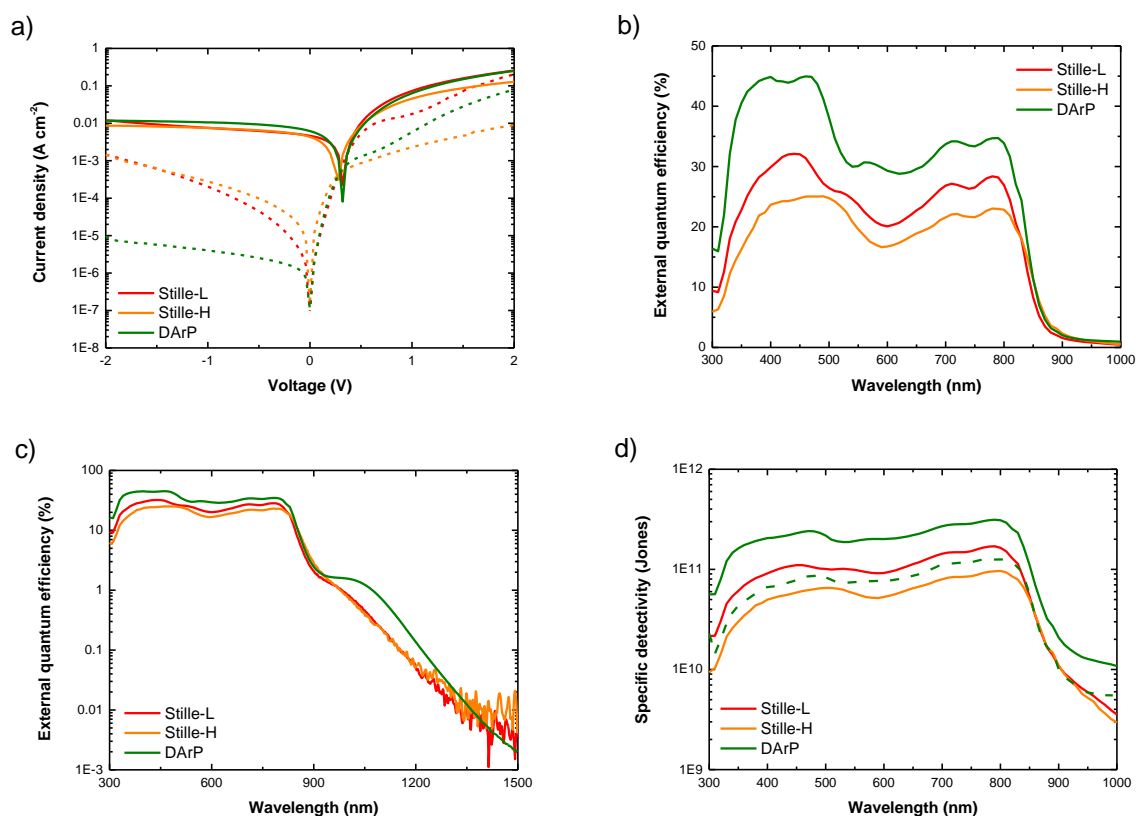


Figure 3 (a) $J - V$ curves measured under illumination (full lines) and in the dark (dashed lines) for the optimized OPD devices based on the Stille-L (red), Stille-H (orange), and DArP (green) polymer in (1:4) blends with PC₆₁BM. (b) EQE spectra, measured at 0 V. (c) Logarithmic plot of the sensitive EQE, measured at 0 V. (d) Calculated specific detectivities at -0.1 V (full lines) and at -2 V (dashed line).

To achieve a better understanding on the varying performance of the Stille vs. DArP PDTPQx, the active layer blends are investigated with atomic force microscopy (AFM). **Figure 4** shows the topography of the optimized material blends, visualizing similar surface roughness and no clear signs of extensive phase separation in any of the blends. From these images, it is clear that no large differences in surface topography exist between the optimized material blends. However, a large difference between the reference samples (processed without solvent additive) vs. the samples processed with DIO is observed (**Figure S15-S20**). The AFM images of the reference samples indicate some phase separation, potentially increasing J_D and decreasing the EQE, as poorly mixed donor:acceptor blends are unfavorable for photocurrent generation and might induce shunt pathways for charge carriers through the neat phases.³⁶

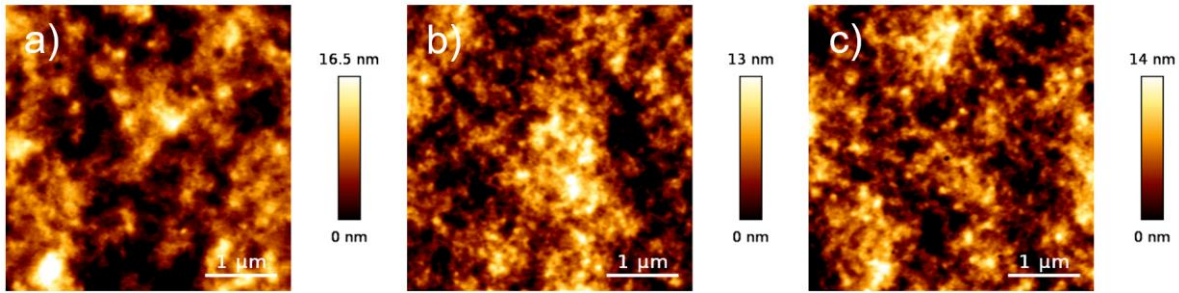


Figure 4 AFM images of optimized PDTPQx:PC₆₁BM (1:4) active layers processed from chloroform with DIO (5 v/v%) based on the (a) Stille-L, (b) Stille-H, and (c) DArP polymer.

Since AFM does not clarify the extensive difference in J_D between the optimized devices, transmission electron microscopy (TEM) measurements are additionally performed (**Figure 5**). From these measurements, it is clear that all material blends are amorphous (diffraction patterns are shown in **Figure S21-S26**). A small difference in morphology can be observed between the Stille-L active layer on the one hand, and the Stille-H and DArP active layers on the other hand, as somewhat larger domains exist in the Stille-L blend. This distinction probably originates from the molar mass variation of the polymers. No apparent differences in morphology between the Stille-H and DArP blends are observed. Similar to the AFM measurements, a significant difference between the reference samples vs. the samples processed with DIO is seen (**Figure S21-S26**), again stressing the morphological benefit of the use of solvent additives. However, the differences in J_D and EQE can not be explained based on these microscopy results.

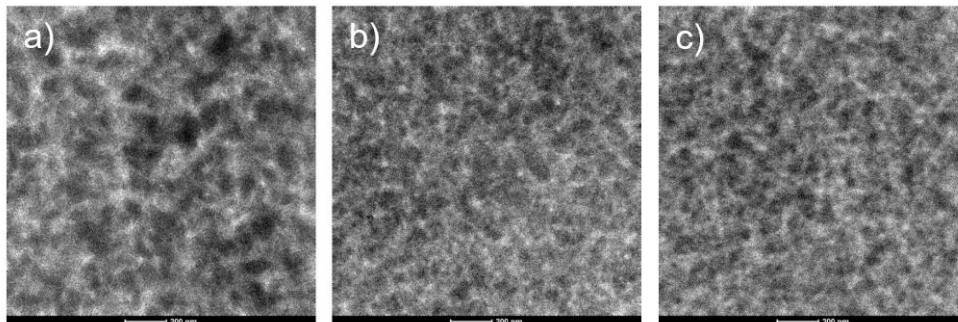


Figure 5 TEM images of optimized PDTPQx:PC₆₁BM (1:4) active layers processed from chloroform with DIO (5 v/v%) based on the (a) Stille-L, (b) Stille-H, and (c) DArP polymer batch.

Because of the distinct CT band observed in the 950 to 1150 nm region for the DArP PDTPQx:PC₆₁BM (1:4) blend (**Figure 3c**), a resonant optical cavity photodetector is fabricated for this blend. This particular type of photodetector lends itself to wavelength selective photodetection at the tunable resonance wavelengths.^{6, 29} For a Fabry-Pérot cavity, the resonance wavelength is proportional to both the cavity thickness and the effective refractive index of the photoactive layer.^{37, 38} The cavity device stack consists of the DArP PDTPQx:PC₆₁BM (1:4) active layer blend processed from chloroform with solvent additive DIO (5 v/v%), with PEIE as electron transport layer and MoO₃ as hole transport layer, sandwiched between a thick non-transparent and a thin semi-transparent Ag electrode on a glass substrate. All details about the cavity OPD fabrication can be found in the SI. For the devices with a 180 nm and a 210 nm thick BHJ active layer (**Figure 6**), EQEs of 2.5% at 1016 nm and 1% at 1140 nm are achieved with rather narrow peak responses with a full-width-at-half-maximum (FWHM) of 44 and 45 nm, respectively, and specific detectivities of 2.24×10^{10} and 1.06×10^{10} Jones (calculated at -0.1 V) (**Table S2**). For all PDTPQx:PC₆₁BM (1:4) based devices, an undulating surface was observed when monitoring the blend thickness with a profilometer. Future optimization of the blend surface

morphology and homogeneity of the blend thickness, directly linked to the EQE and FWHM in an optical cavity OPD,³¹ could possibly further enhance the detectivities.

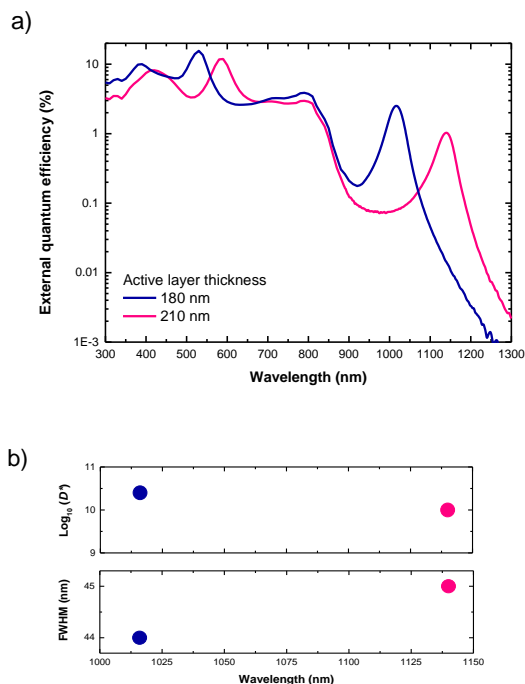


Figure 6 (a) EQEs of the optical resonant cavity OPD based on the DARp PDTPQx:PC₆₁BM (1:4) blend, with active layer thicknesses of 180 nm (in blue) and 210 nm (in pink). (b) Calculated detectivities (at -0.1 V) and FWHM values of the resonance peaks between 1000 and 1150 nm.

3. Conclusions

The high-HOMO polymer PDTPQx is synthesized *via* both Stille polycondensation and (the more sustainable alternative) direct arylation polymerization, yielding three polymers named Stille-L, Stille-H, and DARp. Near-infrared organic photodetectors are constructed based on these different polymer batches, and their performances are investigated. The ITO/PEIE/PDTPQx:PC₆₁BM(1:4)/MoO₃/Ag device stack, with the active layer blend processed from chloroform with solvent additive DIO (5 v/v%), shows the best overall results. From the $J - V$ characteristics it is clear that the DARp-based devices outperform the Stille-based devices. Only the DARp-based device shows a clear charge-transfer absorption band in the sensitively measured EQE spectrum. Furthermore, specific detectivities at -2 V are calculated, only for the DARp-based device, as the dark current of the Stille-based devices is too high and dominated by noise. Because of the distinct charge-transfer absorption band of the DARp-based device, optical resonant cavity OPDs are made for that specific material blend. Those devices show peak EQEs of 2.5% and 1% at resonance wavelengths of 1016 and 1140 nm, with full-width-at-half-maximum peak responses of 44 and 45 nm and detectivities of 2.24×10^{10} and 1.06×10^{10} Jones, respectively. The origin of the performance gap between the devices based on the Stille polymers on the one hand, and the DARp polymer on the other hand, remains unknown for now. AFM and TEM measurements indicate no substantial differences in topography and bulk morphology, respectively. Comparing Stille-H and DARp, the similar melting enthalpy also indicates a similar degree of crystallinity. Whereas the high-temperature NMR spectra of the highest molar mass Stille and the DARp polymer are very similar, MALDI-ToF mass spectrometry reveals that the main difference between the different polymers is in the end groups, which are not expected to play such a crucial role. In any case, this once again illustrates that there is still much to learn on the effect of subtle structural variations

of push-pull conjugated polymers on their performance in organic electronic devices, and further efforts in this direction are certainly required.^{19, 20}

Acknowledgements

The authors thank Huguette Penxten for CV analysis, Christel Willems for the TEM sample preparation, and Brent Fripont for the graphical abstract artwork. We also thank the Research Foundation – Flanders (FWO Vlaanderen) for continuing financial support (projects GOD0118N, GOB2718N, 1S50820N, 11D2618N), as well as the European Research Council (ERC, grant agreement 864625). Dr. Q. Liu acknowledges financial support from the European Union's Horizon 2020 research and innovation program under the Marie-Curie grant agreement no. 88279.

References

1. Ostroverkhova, O., Organic Optoelectronic Materials: Mechanisms and Applications. *Chemical Reviews* **2016**, *116*, 13279-13412.
2. Pankow, R. M.; Thompson, B. C., The development of conjugated polymers as the cornerstone of organic electronics. *Polymer* **2020**, *207*, 122874.
3. Wang, T.; Kupgan, G.; Brédas, J.-L., Organic Photovoltaics: Relating Chemical Structure, Local Morphology, and Electronic Properties. *Trends in Chemistry* **2020**, *2*, 535-554.
4. Pode, R., Organic light emitting diode devices: An energy efficient solid state lighting for applications. *Renewable and Sustainable Energy Reviews* **2020**, *133*, 110043.
5. Ren, H.; Chen, J.-D.; Li, Y.-Q.; Tang, J.-X., Recent Progress in Organic Photodetectors and their Applications. *Advanced Science* **2021**, *8*, 2002418.
6. Vanderspikken, J.; Maes, W.; Vandewal, K., Wavelength-Selective Organic Photodetectors. *Advanced Functional Materials* **2021**, *31*, 2104060.
7. Kim, M.; Ryu, S. U.; Park, S. A.; Choi, K.; Kim, T.; Chung, D.; Park, T., Donor–Acceptor-Conjugated Polymer for High-Performance Organic Field-Effect Transistors: A Progress Report. *Advanced Functional Materials* **2020**, *30*, 1904545.
8. Rivnay, J.; Inal, S.; Salleo, A.; Owens, R. M.; Berggren, M.; Malliaras, G. G., Organic electrochemical transistors. *Nature Reviews Materials* **2018**, *3*, 17086.
9. Bronstein, H.; Nielsen, C. B.; Schroeder, B. C.; McCulloch, I., The role of chemical design in the performance of organic semiconductors. *Nature Reviews Chemistry* **2020**, *4*, 66-77.
10. Carsten, B.; He, F.; Son, H. J.; Xu, T.; Yu, L., Stille Polycondensation for Synthesis of Functional Materials. *Chemical Reviews* **2011**, *111*, 1493-1528.
11. Sakamoto, J.; Rehahn, M.; Wegner, G.; Schlüter, A. D., Suzuki Polycondensation: Polyarylenes à la Carte. *Macromolecular Rapid Communications* **2009**, *30*, 653-687.
12. Osaka, I.; McCullough, R. D., Advances in Molecular Design and Synthesis of Regioregular Polythiophenes. *Accounts of Chemical Research* **2008**, *41*, 1202-1214.
13. Chen, T.-A.; Wu, X.; Rieke, R. D., Regiocontrolled Synthesis of Poly(3-alkylthiophenes) Mediated by Rieke Zinc: Their Characterization and Solid-State Properties. *Journal of the American Chemical Society* **1995**, *117*, 233-244.
14. Alberico, D.; Scott, M. E.; Lautens, M., Aryl–Aryl Bond Formation by Transition-Metal-Catalyzed Direct Arylation. *Chemical Reviews* **2007**, *107*, 174-238.
15. Gobalasingham, N. S.; Thompson, B. C., Direct arylation polymerization: A guide to optimal conditions for effective conjugated polymers. *Progress in Polymer Science* **2018**, *83*, 135-201.
16. Di Mauro, E.; Rho, D.; Santato, C., Biodegradation of bio-sourced and synthetic organic electronic materials towards green organic electronics. *Nature Communications* **2021**, *12*, 3167.
17. Tropp, J.; Rivnay, J., Design of biodegradable and biocompatible conjugated polymers for bioelectronics. *Journal of Materials Chemistry C* **2021**, *9*, 13543.
18. Ponder Jr, J. F.; Chen, H.; Luci, A. M. T.; Moro, S.; Turano, M.; Hobson, A. L.; Collier, G. S.; Perdigão, L. M. A.; Moser, M.; Zhang, W.; Costantini, G.; Reynolds, J. R.; McCulloch, I., Low-Defect, High

Molecular Weight Indacenodithiophene (IDT) Polymers Via a C–H Activation: Evaluation of a Simpler and Greener Approach to Organic Electronic Materials. *ACS Materials Letters* **2021**, 1503-1512.

19. Qiu, Z.; Hammer, B. A. G.; Müllen, K., Conjugated polymers – Problems and promises. *Progress in Polymer Science* **2020**, *100*, 101179.
20. Pirotte, G.; Verstappen, P.; Vanderzande, D.; Maes, W., On the “True” Structure of Push–Pull-Type Low-Bandgap Polymers for Organic Electronics. *Advanced Electronic Materials* **2018**, *4*, 1700481.
21. Vangerven, T.; Verstappen, P.; Drijkoningen, J.; Dierckx, W.; Himmelberger, S.; Salleo, A.; Vanderzande, D.; Maes, W.; Manca, J. V., Molar Mass versus Polymer Solar Cell Performance: Highlighting the Role of Homocouplings. *Chemistry of Materials* **2015**, *27*, 3726-3732.
22. Rasmussen, S. C.; Evenson, S. J., Dithieno[3,2-b:2',3'-d]pyrrole-based materials: Synthesis and application to organic electronics. *Progress in Polymer Science* **2013**, *38*, 1773-1804.
23. Geng, Y.; Tang, A.; Tajima, K.; Zeng, Q.; Zhou, E., Conjugated materials containing dithieno[3,2-b:2',3'-d]pyrrole and its derivatives for organic and hybrid solar cell applications. *Journal of Materials Chemistry A* **2019**, *7*, 64-96.
24. Vanormelingen, W.; Kesters, J.; Verstappen, P.; Drijkoningen, J.; Kudrjasova, J.; Koudjina, S.; Liégeois, V.; Champagne, B.; Manca, J.; Lutsen, L.; Vanderzande, D.; Maes, W., Enhanced open-circuit voltage in polymer solar cells by dithieno[3,2-b:2',3'-d]pyrrole N-acylation. *Journal of Materials Chemistry A* **2014**, *2*, 7535-7545.
25. Kesters, J.; Verstappen, P.; Vanormelingen, W.; Drijkoningen, J.; Vangerven, T.; Devisscher, D.; Marin, L.; Champagne, B.; Manca, J.; Lutsen, L.; Vanderzande, D.; Maes, W., N-acyl-dithieno[3,2-b:2',3'-d]pyrrole-based low bandgap copolymers affording improved open-circuit voltages and efficiencies in polymer solar cells. *Solar Energy Materials and Solar Cells* **2015**, *136*, 70-77.
26. Raymakers, J.; Haenen, K.; Maes, W., Diamond surface functionalization: from gemstone to photoelectrochemical applications. *Journal of Materials Chemistry C* **2019**, *7*, 10134-10165.
27. Gedefaw, D.; Prosa, M.; Bolognesi, M.; Seri, M.; Andersson, M. R., Recent Development of Quinoxaline Based Polymers/Small Molecules for Organic Photovoltaics. *Advanced Energy Materials* **2017**, *7*, 1700575.
28. Siegmund, B.; Mischok, A.; Benduhn, J.; Zeika, O.; Ullbrich, S.; Nehm, F.; Böhm, M.; Spoltore, D.; Fröb, H.; Körner, C.; Leo, K.; Vandewal, K., Organic narrowband near-infrared photodetectors based on intermolecular charge-transfer absorption. *Nature Communications* **2017**, *8*, 15421.
29. Tang, Z.; Ma, Z.; Sánchez-Díaz, A.; Ullbrich, S.; Liu, Y.; Siegmund, B.; Mischok, A.; Leo, K.; Campoy-Quiles, M.; Li, W.; Vandewal, K., Polymer:Fullerene Bimolecular Crystals for Near-Infrared Spectroscopic Photodetectors. *Advanced Materials* **2017**, *29*, 1702184.
30. Kaiser, C.; Schellhammer, K. S.; Benduhn, J.; Siegmund, B.; Tropiano, M.; Kublitski, J.; Spoltore, D.; Panhans, M.; Zeika, O.; Ortmann, F.; Meredith, P.; Armin, A.; Vandewal, K., Manipulating the Charge Transfer Absorption for Narrowband Light Detection in the Near-Infrared. *Chemistry of Materials* **2019**, *31*, 9325-9330.
31. Vanderspikken, J.; Liu, Q.; Liu, Z.; Vandermeeren, T.; Cardeynals, T.; Gielen, S.; Van Mele, B.; Van den Brande, N.; Champagne, B.; Vandewal, K.; Maes, W., Tuning Electronic and Morphological Properties for High-Performance Wavelength-Selective Organic Near-Infrared Cavity Photodetectors. *Advanced Functional Materials* **2021**, *31*, 2108146.
32. Mishra, S. P.; Palai, A. K.; Srivastava, R.; Kamalasanan, M. N.; Patri, M., Dithieno[3,2-b:2',3'-d]pyrrole–alkylthiophene–benzo[c][1,2,5]thiadiazole-based highly stable and low band gap polymers for polymer light-emitting diodes. *Journal of Polymer Science Part A: Polymer Chemistry* **2009**, *47*, 6514-6525.
33. Marin, L.; Lutsen, L.; Vanderzande, D.; Maes, W., Quinoxaline derivatives with broadened absorption patterns. *Organic & Biomolecular Chemistry* **2013**, *11*, 5866-5876.
34. Wakioka, M.; Torii, N.; Saito, M.; Osaka, I.; Ozawa, F., Donor–Acceptor Polymers Containing 4,8-Dithienylbenzo[1,2-b:4,5-b']dithiophene via Highly Selective Direct Arylation Polymerization. *ACS Applied Polymer Materials* **2021**, *3*, 830-836.
35. Spoltore, D.; Vangerven, T.; Verstappen, P.; Piersimoni, F.; Bertho, S.; Vandewal, K.; Van den Brande, N.; Defour, M.; Van Mele, B.; De Sio, A.; Parisi, J.; Lutsen, L.; Vanderzande, D.; Maes, W.;

- Manca, J. V., Effect of molecular weight on morphology and photovoltaic properties in P3HT:PCBM solar cells. *Organic Electronics* **2015**, *21*, 160-170.
36. Verstraeten, F.; Gielen, S.; Verstappen, P.; Kesters, J.; Georgitzikis, E.; Raymakers, J.; Cheyns, D.; Malinowski, P.; Daenen, M.; Lutsen, L.; Vandewal, K.; Maes, W., Near-infrared organic photodetectors based on bay-annulated indigo showing broadband absorption and high detectivities up to 1.1 μm . *Journal of Materials Chemistry C* **2018**, *6*, 11645-11650.
37. Ünlü, M. S.; Strite, S., Resonant cavity enhanced photonic devices. *Journal of Applied Physics* **1995**, *78*, 607-639.
38. Liu, Q.; Toudert, J.; Li, T.; Kramarenko, M.; Martínez-Denegri, G.; Ciammaruchi, L.; Zhan, X.; Martorell, J., Inverse Optical Cavity Design for Ultrabroadband Light Absorption Beyond the Conventional Limit in Low-Bandgap Nonfullerene Acceptor-Based Solar Cells. *Advanced Energy Materials* **2019**, *9*, 1900463.